UNIVERSITY OF SÃO PAULO

INSTITUTE OF GEOSCIENCES

On the evolution of alkali ultrabasic to intermediate magmatism: insights from experimental petrology and geochemistry

ANDRÉS FABIÁN SALAZAR NARANJO

Thesis presented to the program of the Geosciences (Mineralogy and Petrology) for the degree of Doctor of Sciences

Area: Igneous and Metamorphic Petrology

Advisor: Prof. Dr. Silvio Roberto Farias Vlach

SÃO PAULO

2023

Autorizo a reprodução e divulgação total ou parcial deste trabalho, por qualquer meio convencional ou eletrônico, para fins de estudo e pesquisa, desde que citada a fonte.

Serviço de Biblioteca e Documentação do IGc/USP
Ficha catalográfica gerada automaticamente com dados fornecidos pelo(a) autor(a)
via programa desenvolvido pela Seção Técnica de Informática do ICMC/USP

Bibliotecários responsáveis pela estrutura de catalogação da publicação:
Sonia Regina Yole Guerra - CRB-8/4208 | Anderson de Santana - CRB-8/6658

Salazar Naranjo, Andrés Fabián On the evolution of alkali ultrabasic to intermediate magmatism: insights from experimental petrology and geochemistry / Andrés Fabián Salazar Naranjo; orientador Silvio Roberto Farias Vlach. -São Paulo, 2023.
233 p.

Tese (Doutorado - Programa de Pós-Graduação em Mineralogia e Petrologia) -- Instituto de Geociências, Universidade de São Paulo, 2023.

1. Experimental petrology and geochemistry. 2. Intensive parameters. 3. Alkali magma series. 4. Titanian Ca-clinopyroxene. I. Farias Vlach, Silvio Roberto, orient. II. Título.

UNIVERSIDADE DE SÃO PAULO
INSTITUTO DE GEOCIÊNCIAS

On the evolution of alkali ultrabasic to intermediate magmatism: insights from experimental petrology and geochemistry

ANDRES FABIAN SALAZAR NARANJO

Orientador: Prof. Dr. Silvio Roberto Farias Vlach

Tese de Doutorado

Nº 664

COMISSÃO JULGADORA

Dr. Silvio Roberto Farias Vlach

Dr. Guilherme Mallmann

Dr. Daniele Giordano

Dra. Fernanda Gervasoni

Dr. Rommulo Vieira da Conceição

SÃO PAULO
2023

ACKNOWLEDGEMENTS

At the end of almost 9 years at USP, I would like to express my gratitude and respect to my supervisor Silvio Vlach, for his patient support and advice amid the many uncertainties and variables that arose throughout this challenging research. Thanks for this opportunity, I hope that the scientific collaboration can continue in future projects.

I am extremely grateful to Claudio for his immeasurable support as boyfriend, friend, and colleague. You represented all-in-one. Our adventure together is still ongoing. I'm really glad for the opportunity to introduce to my life very important people that I consider my family. You have been on all this journey Katya, Martín, Rodolfo, Melina, Atila, Fares, Caetano, Erika, and Eliana. Thanks for the many amazing moments, laughs and diverse alcoholic drinks!

I would like to thank to Maria Isabel and Astrid for their unconditional support even in the distance. True friendship has no boundaries. Special thanks to all the new friends that Brazil gave me including Alice, Adriana (Bis), Sheila (Ser), Rafael (Vivih), Clarissa, Tainá, Camila, Mary, Pedro (Porra), Cleber, Maria Paula, Yoyis, Santiago, Natalia, Paula, Daniel, Verito, Sebastian, Diego, Anita, Caro, Lina, Barbara, Mikaella (Grega), Debora, Eliana, Fernanda, Nadia and Allan.

Thanks to my family, especially my mothers (Lola and Emma), my niece (Majo), my sister (Maria Aleja and Andreita) for supporting me in my decisions even if it separates us. Notably, I would like to express how much I miss you, my brother (Wilson), and my aunt (Tilita), all of whom I sadly lost during this period.

Bernard Wood thank you for taking the time and for your insightful feedback during a short academic visit to the University of Oxford.

Finally, I would like to thank the São Paulo Research Foundation (FAPESP) for funding this research through my doctorate fellowship (Proc. 2018/16755-4) and the project grant to V. Janasi (2019/22084-8). I equally would like to express my gratitude to the staff of the GeoAnalítica and Technological Characterization Lab Multiuser Centers at the University of Sao Paulo, particularly Artur Takashi Onoe, Marcos Mansueto, Vinicius Martins and Liz Zanchetta.

“I can almost see it

That dream I'm dreaming

But there's a voice inside my head saying

You'll never reach it

Every step I'm taking

Every move I make feels

Lost with no direction

My faith is shaking

But I, I gotta keep trying

Gotta keep my head held high

There's always gonna be another mountain

I'm always gonna wanna make it move

Always gonna be an uphill battle

Sometimes I'm gonna have to lose

Ain't about how fast I get there

Ain't about what's waiting on the other side

It's the climb”

Miley Cyrus

ABSTRACT

Two alkali ultrabasic compositions from the Meso-Cenozoic Serra do Mar Alkaline Province dike swarm were geochemically and mineralogically characterized and used as starting materials in crystallization experiments to constrain the evolution of alkali ultrabasic to intermediate magmas and their crystalline phases close to equilibrium under a wide range of physicochemical parameters. The first sample corresponds to a basanite with sodic affinity, its composition is close to primary magmas (Mg#=63) and enriched in LILE, HFSE, and REE relative to the primitive mantle. Its mineralogy comprises olivine macrocrysts in a fined-grained groundmass of olivine, clinopyroxene, spinel, and alkali-feldspar. The second sample is a tephrite (olivine-free) with potassic affinity, which has a Mg#=48 and shows clinopyroxene macrocrysts in a fined-grained groundmass of clinopyroxene, spinel, and plagioclase. The crystallization experiments were performed at one-atmosphere pressure (100kPa) and from low- to high-pressure (0.5-2.0 GPa). Under 100 kPa, experiments were carried out over a range of fO_2, from 2 log units below to 2 log units above the fayalite-magnetite-quartz buffer (QFM), using a high-temperature vertical furnace with CO/CO_2 gas mixture. The low- to high-pressure experiments were conducted in an end-loaded piston-cylinder using a Pt-graphite capsule (CCO buffer) and NaCl-pyrex-graphite-MgO assemblage. The melts present different compositional paths. For basanite, a sodic and strongly SiO_2-undersaturated liquid line of descent (basanite-tephrite-phonotephrite-tephriphonolite) is derived. For tephrite, it is sodic-potassic/potassic and weakly SiO_2-undersaturated (tephrite-alkali-basalt-phonotephrite) or SiO_2-saturated (tephrite-trachybasalt-trachyandesite), under reduced or oxidized conditions, respectively. Based on the percentages of experimental glasses, we concluded that evolved sodic magmas can be derived from the crystal fractionation of basanite. The iron-magnesium exchange coefficients between mafic silicate minerals and alkali melts ($Kd_{Fe^{2+}-Mg}^{Xtl-Alkali\ melt}$) are slightly lower than those observed in tholeiitic melts, with values of 0.29±0.02 for olivine and 0.25±0.02 for clinopyroxene. In both starting compositions, the crystallized clinopyroxenes are Ti- and Al-rich, and Si-poor, with a compositional trend of evolution from Mg-rich augite to ferroan diopside. Thermobarometric proxies such as MgO-in-melts and clinopyroxene-composition were improved for application in alkali ultrabasic to intermediate rocks, following the equations: $T\ (\pm 5°C) = 27.35\ (MgO^{liq}) + 984$, for one-atmosphere pressure and anhydrous conditions and, $P(\pm 1.4\ kbar) = 160.20Na - 80.68Ti - 17.68Fe^{3+} + 6.36$, where Na, Ti, and Fe^{3+} are cationic proportions relative to 6O of clinopyroxene. The trace element partitioning between

titanian Ca-clinopyroxene and alkali melts was also studied, which might allow petrologists and geochemists to better investigate the genesis and evolution of alkali igneous rocks. The trace elements studied here were first-row transition metals, lithium, large ion lithophile elements, high-field strength elements, and rare earth elements. The results show that P-T-fO_2 strongly influences the behavior of trivalent cations, in both M1 and M2 sites. $D_{HFSE}^{Cpx/melt}$ and $D_{REE}^{Cpx/melt}$ vary following the compositional trend of the evolution of cpx and their substitution is in agreement with Tschermakite-type. The lattice-strain model successfully fitted the divalent and trivalent cation on the M2 site. The Wood and Blundy (1997) and Sun and Liang (2012) models that predict the REE partitioning between clinopyroxene and silicate melt do not predict the negative correlations between $D_{REE}^{Cpx/melt}$ and pressure. However, the Wood and Blundy (1997) model based on activities for $Na_{0.5}(REE)_{0.5}MgSi_2O_6$ component efficiently reproduces the partitioning of REE under 100 kPa. Finally, clinopyroxene is capable of fractionating the U/Th ratio, but Zr/Hf and Ta/Nb are not.

Keywords: experimental petrology and geochemistry; intensive parameters; alkali magma series; titanian Ca-clinopyroxene.

RESUMO

Duas composições alcalinas ultrabásicas do enxame de diques da Província Alcalina Meso-Cenozóica Serra do Mar foram caracterizadas geoquímica e mineralogicamente e usadas como materiais de partida em experimentos de cristalização para examinar a evolução de magmas ultrabásicos a intermediários alcalinos e suas fases cristalinas em equilíbrio sob uma ampla faixa de parâmetros físico-químicos. A primeira amostra corresponde a um basanito com afinidade sódica, sua composição é próxima a magmas primários (Mg# = 63) e enriquecida em LILE, HFSE e REE em relação ao manto primitivo. Sua mineralogia compreende macrocristais de olivina em uma matriz de granulação fina de olivina, clinopiroxênio, espinélio e feldspato alcalino. A segunda amostra é um tefrito (sem olivina) com afinidade potássica, com Mg# = 48 e apresenta macrocristais de clinopiroxênio em uma matriz de granulação fina de clinopiroxênio, espinélio e plagioclásio. Simulações de cristalização foram realizadas sob pressão atmosférica (100kPa) e sob baixas a altas pressões (0.5-2.0 GPa). Sob 100 kPa, os experimentos foram realizados em uma faixa de fugacidades de O_2 (fO_2), desde 2 unidades logarítmicas abaixo até 2 unidades logarítmicas acima do tampão fayalita-magnetita-quartzo (QFM), usando um forno vertical de alta temperatura acoplado com sistema de mistura de gases CO/CO_2. Os experimentos de baixa a alta pressão foram conduzidos em um pistão-cilindro usando uma cápsula de Pt-grafite (tampão CCO) e uma assembleia de NaCl-pirex-grafite-MgO. Os fundidos apresentam diferentes trajetórias composicionais. A partir do basanito, uma *liquid line of descent* (*lld*) sódica e fortemente insaturada em SiO_2 (basanito-tefrito-fonotefrito-tefrifonolito) é derivada. A partir do tefrito, obteve-se *llds* sódico-potássicas/potássicas, levemente insaturada em SiO_2 (tefrito-álcali-basalto-fonotefrito) a saturada em SiO_2 (tefrito-traquibasalto-traquiandesito), sob condições reduzidas e oxidadas, respectivamente. Com base nas porcentagens de vidros experimentais resultantes, conclui-se que quantidades significativas de magmas sódicos podem ser derivados por fracionamento de magmas originais basaníticos. Os coeficientes de troca ferro-magnésio entre minerais silicáticos máficos e fusões alcalinas ($Kd_{Fe^{2+}-Mg}^{Xtl-Alkali\ melt}$) são ligeiramente inferiores aos observados em fusões toleíticas, com valores de 0.29±0.02 para olivina e 0.25±0.02 para clinopiroxênio. Em ambas as composições iniciais, os clinopiroxênios cristalizados são ricos em Ti e Al, e pobres em Si, com uma trajetória composicional de evolução de augita rica em Mg para diopsídio ferroano. Indicadores termobarométricos como MgO-em-vidro e composição de clinopiroxênio foram aprimorados para aplicação em rochas alcalinas ultrabásicas a intermediárias, obtendo-se respectivamente as calibrações:

$T\ (\pm 5°C) = 27.35\ (MgO^{liq}) + 984$ para pressão atmosférica e condições anidras e, $P(\pm 1.4\ kbar) = 160.20Na - 80.68Ti - 17.68Fe^{3+} + 6.36$ para todo o intervalo experimental investigado, onde Na, Ti e Fe3+ são as proporções catiônicas relativas a 6O do clinopiroxênio. A partição de elementos traços entre titano clinopiroxênio cálcico e fusões alcalinas também foi estudada, resultando em valores otimizados que permitem modelamentos geoquímicos mais apropriados para a gênese e evolução das séries alcalinas. Os elementos traços investigados incluíram metais de transição da primeira série, lítio, elementos de baixo potencial iônico (litófilos, LILE), elementos de alto potencial iônico (HFSE) e os elementos de terras raras (REEs, incluindo Y). Os resultados mostram que os parâmetros P-T-fO_2 influenciam fortemente o comportamento dos cátions trivalentes, tanto no sítio M1 quanto no M2. $D_{HFSE}^{Cpx/melt}$ e $D_{REE}^{Cpx/melt}$ variam seguindo a trajetória composicional da evolução dos clinopiroxênios de acordo principalmente com uma substituição heterovalente de tipo tschermakita. O *lattice-strain model* ajusta muito bem os cátions divalentes e trivalentes no sítio M2. Os modelos de Wood e Blundy (1997) e Sun e Liang (2012) que preveem a partição dos REEs entre clinopiroxênio e fusões silicáticas não preveem as correlações negativas entre $D_{REE}^{Cpx/melt}$ e pressão. O modelo de Wood e Blundy (1997), baseado nas atividades do componente $Na_{0.5}(REE)_{0.5}MgSi_2O_6$, reproduz muito bem a partição do REE sob 100 kPa. Finalmente, os titano clinopiroxênios cálcicos são capazes de fracionar significativamente as razões U/Th, mas não as razões Zr/Hf e Ta/Nb.

Palavras-chave: Petrologia e geoquímica experimentais; parâmetros intensivos; serie magmática alcalina; titano clinopiroxênio cálcico.

CONTENTS

1. INTRODUCTION

Experimental petrology and geochemistry have historically contributed with a rich source of fundamental information to geosciences and have been essential to the development of millimeter-to-kilometer scale models of the Earth´s origin and evolution. Most igneous rock investigations now incorporate experimental insights to solve petrological problems from field to mineral scales through the use of geochemical and/or thermodynamical data (Yoder, 1998; Shaw, 2018). The differentiation of basaltic magmas through fractional crystallization processes and compositional changes in crystals (e.g., zonation and solid solution) and melts is a classic example of how experimental petrology provided a long-standing contribution to the interpretation of natural and more complex scenarios. The comprehension of these mechanisms were firstly acquired from Bowen's (1915) experimental results using a simple chemical system (diopside-albite-anorthite). Another key example of the understanding of basalt genesis is the experimental work performed by Jaques and Green (1980) just above the *solidus* in the pressure range 0-15 kb with peridotite (pyrolite and spinel lherzolite). They demonstrated the relationship between the transition in melt composition with increasing pressure, from quartz tholeiite to tholeiitic picrite, and with melting percentage, from alkali olivine basalt (<15%) through olivine tholeiite (20-30%) to komatiite (40~50%). Hence, experiments carried out in laboratory are key procedures to simulate mineralogical, petrological, and geochemical processes in order to better understand the physical and chemical features and relationships of minerals, rocks, melts, and fluids (Geiger and Kawamoto, 2017).

In geochemical terms, alkali magmas are distinguished from subalkali magmas (e.g., tholeiitic basalt) by their high concentrations of alkalis, trace elements, and volatiles (such as CO_2 and H_2O) (Gast, 1968), and this behavior, coupled to isotopic compositions, has been used to argue for chemical heterogeneity within the Earth's mantle (Allègre and Minster, 1978; Hofmann, 1997). Nonetheless, the petrological mechanisms responsible for the formation of alkali magmas are still being debated, and numerous models have been proposed, mainly based on experimental petrology. For example, the genesis of alkali magmas is usually explained as: (1) low-degree melting of garnet peridotite in presence of H_2O or CO_2 (Green, 1973; Gaetani and Grove, 1998; Dasgupta et al., 2007); (2) partial melting of garnet pyroxenite that represents the interaction between recycled subducted oceanic crust and mantle peridotite (Hirschmann et al., 2003; Kogiso et al., 2003) or (3) melts

from metasomatized lithospheric mantle, where melting of phlogopite- or amphibole-bearing metasomatic veins interact with the surrounding mantle to generate potassic or sodic magmas, respectively (Foley, 1992; Pilet et al., 2008a).

Among the diverse experimental investigations that have been conducted to examine the generation of alkali basaltic magmas, only a few experimental studies are available to outline the evolution of these magmas from their origin to their emplacement (e.g., Nekvasil et al., 2004; Scoates et al., 2006; Pilet et al., 2010). One of the most significant mechanisms influencing the geochemical evolution of basaltic liquids is fractional crystallization, however, there are other petrological processes acting in either close- or open-systems (O'Hara, 1977; Pankhurst, 1977). Trace elements are very useful to recognize and model any of these possibilities. In both cases, generation and evolution, the distribution of trace elements in alkali magmas is highly sensitive to the presence of different phases (silicates and fluids), and intensive parameters, such as pressure (P), temperature (T) and oxygen fugacity (fO_2) (e.g., Witt-Eickschen and O'Neill, 2005; De Hoog et al., 2010; Wood and Blundy, 2014). As a result, the partitioning behavior of trace elements, expressed through the Nernst crystal/melt partition coefficients, combined with the geochemical signatures preserved in rocks and minerals through textures, phase distribution, and chemical zonation, is a powerful tool to envision complex natural systems and identify all of these magmatic processes (Blundy and Cashman, 2008; Ghiorso, 2018). Because many physical-chemical parameters must be considered to simulate magmatic processes, selecting the appropriate partition coefficients is crucial to achieve models that are more reliable or closer to natural cases (Wood and Blundy, 2014).

An important advance is that experiments can now be coupled to high-quality microanalysis of experimental products due to improvements in high-resolution in-situ measurements, which have led to a dramatically gain in knowledge of partitioning behavior in recent years from experimental data. The available experimental dataset for alkali ultrabasic to intermediate magmas is restricted, particularly in terms of composition (e.g., basanite and alkali basalt) and oxygen fugacity (e.g., QFM). In this thesis, we report the results of a series of experiments conducted from 100 kPa to 2GPa and temperatures ranging between 1250 and 1000°C on two starting materials, basanite, and tephrite. Also, oxygen fugacity was constrained at one-atmosphere pressures from QFM-2 to QFM+2. These experimental data provide new insights into the crystal and liquid compositions along the liquid line of descent,

phase equilibrium, thermobarometry, and trace element partitioning between titanian Ca-clinopyroxene and alkali ultrabasic to intermediate liquids.

1.1. Objectives

Based on the above motivations, the aims of this thesis were:

- Investigate experimentally the evolution of alkali magma series starting from two ultrabasic composition: basanite and tephrite with sodic and potassic affinities, respectively.
- Assess the influence of pressure (P), temperature (T), and oxygen fugacity (fO_2) on the evolutionary trend of the alkali magma series and their crystalline phases close to equilibrium.
- Compare the equilibrium criteria between alkali and subalkali magmas.
- Evaluate the available thermobarometers for alkali ultrabasic to intermediate systems and improve them for this composition.
- Examine the behavior of trace elements under different P-T-fO_2 conditions.
- Determine partition coefficients of large number of trace elements between titanian Ca-clinopyroxene and alkali melts (basanite and tephrite)
- Compare the results with similar ones in available literature and with the empirical and thermodynamic models of trace elements partitioning between clinopyroxene and silicate melt.
- Generate an experimental dataset that will allow future geochemical modeling of the alkali system from genesis to evolution, particularly for the Brazilian Mesozoic alkaline magmatism, as well as other similar alkali provinces.

1.2. Thesis structure

This thesis is composed of 6 chapters. In *Chapter 1*, I present the main subject and goals of this thesis. *Chapter 2* describes the analytical and experimental methods used to achieve the proposed objectives. *Chapter 3* presents the characterization of staring natural materials used in the experimental runs, which includes whole-rock and mineral geochemistry of major, minor and trace elements. *Chapters 4* and *5* present the main obtained results in a scientific manuscript format. Indeed, the first manuscript was submitted to the Journal of Petrology and the second is under improvement and review for submission to Geochimica et Cosmochimica Acta in the near future.

Chapter 4 comprises the manuscript entitled: “New experimental constraints for the evolution and thermobarometry of alkali ultrabasic to intermediate igneous rocks.” In this study, we show the first results based on the textural and chemical analyses via field emission gun-scanning electron microscope (FEG-SEM) and -electron probe microanalyzer (FEG-EPMA), respectively, of the experimental products. The differentiation trend of the liquids and solid phases is mainly discussed constraining the influence of oxygen fugacity. In addition, we used MgO-in-melts and clinopyroxene composition as thermobarometric proxies, to be specifically applied to the alkali ultrabasic to intermediate igneous rocks.

Chapter 5 contains the manuscript entitled: “Experimental insights on trace elements partitioning between titanian Ca-clinopyroxene and alkali magmas: influence of P-T-fO_2-X.” This is based on the experiments of the first manuscript, but this time using the trace elements composition of the clinopyroxene and glasses, that comprises first-row transition metals (FRTM), large-ion lithophile (LILE), high field-strength (HFSE) and rare earth elements (REE) obtained via laser ablation inductively coupled plasma mass spectrometry (LA-ICP-MS). The controls of pressure, temperature, oxygen fugacity, and composition on the partitioning behavior for each geochemical group are discussed. Also, the empirical and thermodynamic models available in the literature were tested and compared with the observed experimental data to see their applicability in alkali ultrabasic to intermediate systems.

Finally, *Chapter 6* covers the final remarks in a brief integrative conclusion of the thesis.

Appendix from A to G contain the data obtained via FEG-SEM, FEG-EPMA, LA-ICP-MS of starting materials and experimental products, as well as the experimental partition coefficients calculated in this study.

1.3. References

Allègre, C.J., and Minster, J.F., 1978, Quantitative models of trace element behavior in magmatic processes: Earth and Planetary Science Letters, v. 38, p. 1–25, doi:10.1016/0012-821X(78)90123-1.

Blundy, J., and Cashman, K., 2008, Petrologic Reconstruction of Magmatic System Variables and Processes: Reviews in Mineralogy and Geochemistry, v. 69, p. 179–239, doi:10.2138/rmg.2008.69.6.

Bowen, N.L., 1915, The crystallization of haplobasaltic, haplodioritic, and related magmas: American Journal of Science, v. s4-40, p. 161–185, doi:10.2475/ajs.s4-40.236.161.

Dasgupta, R., Hirschmann, M.M., and Smith, N.D., 2007, Partial melting experiments of peridotite + CO2 at 3 GPa and genesis of alkalic ocean island basalts: Journal of Petrology, v. 48, p. 2093–2124, doi:10.1093/petrology/egm053.

Foley, S., 1992, Vein-plus-wall-rock melting mechanisms in the lithosphere and the origin of potassic alkaline magmas: Lithos, v. 28, p. 435–453, doi:10.1016/0024-4937(92)90018-T.

Gaetani, G.A., and Grove, T.L., 1998, The influence of water on melting of mantle peridotite: Contributions to Mineralogy and Petrology, v. 131, p. 323–346, doi:10.1007/s004100050396.

Gast, P.W., 1968, Trace element fractionation and the origin of tholeiitic and alkaline magma types: Geochimica et Cosmochimica Acta, v. 32, p. 1057–1086, doi:10.1016/0016-7037(68)90108-7.

Geiger, C.A., and Kawamoto, T., 2017, Experimental Mineralogy and Petrology, in p. 1–6, doi:10.1007/978-3-319-39193-9_311-2.

Ghiorso, M., 2018, Magmatic Process Modeling, in White, W.M. ed., Encyclopedia of Geochemistry: A Comprehensive Reference Source on the Chemistry of the Earth, Cham, Springer International Publishing, p. 841–853, doi:10.1007/978-3-319-39312-4_242.

Green, D.H., 1973, Conditions of melting of basanite magma from garnet peridotite: Earth and Planetary Science Letters, v. 17, p. 456–465, doi:10.1016/0012-821X(73)90214-8.

Hirschmann, M.M., Kogiso, T., Baker, M.B., and Stolper, E.M., 2003, Alkalic magmas generated by partial melting of garnet pyroxenite: Geology, v. 31, p. 481–484, doi:10.1130/0091-7613(2003)031<0481:AMGBPM>2.0.CO;2.

Hofmann, A.W., 1997, Mantle geochemistry: the message from oceanic volcanism: Nature, v. 385, p. 219–229, doi:10.1038/385219a0.

De Hoog, J.C.M., Gall, L., and Cornell, D.H., 2010, Trace-element geochemistry of mantle olivine and application to mantle petrogenesis and geothermobarometry: Chemical Geology, v. 270, p. 196–215, doi:10.1016/j.chemgeo.2009.11.017.

Jaques, A.L., and Green, D.H., 1980, Anhydrous melting of peridotite at 0-15 Kb pressure and the genesis of tholeiitic basalts: Contributions to Mineralogy and Petrology, v. 73, p. 287–310, doi:10.1007/BF00381447.

Kogiso, T., Hirschmann, M.M., and Frost, D.J., 2003, High-pressure partial melting of garnet pyroxenite: Possible mafic lithologies in the source of ocean island basalts: Earth and Planetary Science Letters, v. 216, p. 603–617, doi:10.1016/S0012-821X(03)00538-7.

Nekvasil, H., Dondolini, A., Horn, J., Filiberto, J., Long, H., and Lindsley, D.H., 2004, The origin and evolution of silica-saturated alkalic suites: An experimental study: Journal of Petrology, v. 45, p. 693–721, doi:10.1093/petrology/egg103.

O'Hara, M.J., 1977, Geochemical evolution during fractional crystallisation of a periodically refilled magma chamber: Nature, v. 266, p. 503–507, doi:10.1038/266503a0.

Pankhurst, R.J., 1977, Open system crystal fractionation and incompatible element variation in basalts: Nature, v. 268, p. 36–38, doi:10.1038/268036a0.

Pilet, S., Baker, M.B., and Stolper, E.M., 2008, Metasomatized lithosphere and the origin of alkaline lavas: Science, v. 320, p. 916–919, doi:10.1126/science.1156563.

Pilet, S., Ulmer, P., and Villiger, S., 2010, Liquid line of descent of a basanitic liquid at 1.5 Gpa: Constraints on the formation of metasomatic veins: Contributions to Mineralogy and Petrology, v. 159, p. 621–643, doi:10.1007/s00410-009-0445-y.

Scoates, J.S., Lo Cascio, M., Weis, D., and Lindsley, D.H., 2006, Experimental constraints on the origin and evolution of mildly alkalic basalts from the Kerguelen Archipelago, Southeast Indian

Ocean: Contributions to Mineralogy and Petrology, v. 151, p. 582–599, doi:10.1007/s00410-006-0070-y.

Shaw, C.S.J., 2018, Igneous rock associations 22. Experimental petrology: Methods, examples, and applications: Geoscience Canada, v. 45, p. 67–84, doi:10.12789/geocanj.2018.45.134.

Witt-Eickschen, G., and O'Neill, H.S.C., 2005, The effect of temperature on the equilibrium distribution of trace elements between clinopyroxene, orthopyroxene, olivine and spinel in upper mantle peridotite: Chemical Geology, v. 221, p. 65–101, doi:10.1016/j.chemgeo.2005.04.005.

Wood, B.J., and Blundy, J.D., 2014, Trace Element Partitioning: The Influences of Ionic Radius, Cation Charge, Pressure, and Temperature, in Treatise on Geochemistry, Elsevier, v. 3, p. 421–448, doi:10.1016/B978-0-08-095975-7.00209-6.

Yoder, H.S.J., 1998, Norman L. Bowen: The Experimental Approach to Petrology: GSA Today, v. 5, p. 10–11.

2. MATERIALS AND METHODS

Sample preparation, analytical and experimental procedures were carried out at the laboratories of the GeoAnalitica Multiuser Center, University of São Paulo.

2.1. Preparation of starting materials

The unaltered natural samples used as starting materials were cut and crushed to a size of 1-2 mm using a hydraulic press. Representative aliquots were powdered with an agate mill to obtain particle sizes <200 mesh, and fractions of the obtained powder were double micronized under ethanol using McCrone Micronizer for a total time of 1h to further particle size reduction and powder homogenization.

Basanite was doped with 5 wt% of olivine crystals (Fo~86) as an embryonic phase triggering the nucleation and crystallization of this mineral. This olivine was extracted from itself and picked under a magnifying glass. Additionally, both starting materials were doped with 30 trace elements using standard aqueous solutions from the GeoAnalitica chemical laboratory. The added concentrations were: 100 µg/g for Ni, Cr, V, Co, Zn, Rb, Sr, Ba, Zr, and U; 200 µg/g for Hf, Li, La, Ce, Nd, and Pr; 250 µg/g for Ta; 350 µg/g for Sm, Eu, Gd, Tb, Dy, and Sc; 400 µg/g for Y and 500 µg/g for Ho, Er, Tm, Yb, Lu, and Nb. After doping, samples were dried and further ground under ethanol with an agate mortar for homogenization. A small number of non-doped samples under the same experimental conditions were also tested for comparison purposes and to check for possible effects of the enrichment technique.

2.2.Analytical techniques

2.2.1. Electron microscopy

Textural analysis and identification of the phases in experimental products were performed with backscattered electron (BSE) images and energy-dispersive spectroscopy (EDS) qualitative analysis and compositional mapping. These analyses were carried out with an FEI Quanta 650 FEG field emission scanning electron microscope coupled with a Bruker X-flash 6-60 EDS system under 15 kV for the column accelerating voltage at the Technological Characterization Lab Multiuser Center (LCT) at USP.

2.2.2. Whole-rock analysis

The whole-rock major, minor, and some trace element composition of starting materials were determined using fused glass disc and pressed powder pellet by X-ray Fluorescence (XRF), which were performed in a PANalytical AXIOS MAX advanced spectrometer, following the procedures described by Mori et al. (1999). Also, these starting materials were analyzed via inductively coupled plasma mass spectrometry (ICP-MS) in a Thermo Scientific iCAP Quadrupole equipment, according to the procedures given in Navarro et al. (2008).

2.2.3. Mineral analysis

Major, minor, and some trace element analyses of rock-forming minerals from starting materials as well as experimental products were obtained using a JEOL-8530 field emission gun electron probe microanalyzer (FEG-EPMA), which is equipped with five wavelength-dispersive, one among them provided with large-area PET and TAP analyzer crystals, and one energy-dispersive spectrometers: WDS and EDS, respectively. The analytical conditions are:

- 15 kV accelerating voltage, 20 nA beam current, and 5 µm of spot size for the rock-forming minerals in the starting materials.
- 20 kV accelerating voltage, 20 nA beam current, and 5 µm of spot size for the crystalline phases resulting from the experimental products.
- 20 kV accelerating voltage, 10 nA beam current, and 10 µm of spot size for the glasses resulting from experimental products.

For the analytical WDS setup was employed natural and synthetic standards from the Smithsonian Institution and the Geller^{TM} (McGuire et al., 1992). Count times were equal between on-peak and off-peak. Kα peaks were analyzed for most elements while Lα for Nb, Ba, and Sr. A summary of the analytical procedures and used standards are given in Table *2-1*, Table 2-2, and Table *2-3*. The PRZ/Armstrong software from JEOL was used to correct the matrix effect and convert the raw data to oxide percentages.

The structural formulae for olivine spinel, clinopyroxene, feldspar, biotite, and rhönite were calculated based on 4, 4, 6, 32, 22, and 20 oxygens, respectively. Fe^{2+} and Fe^{3+} proportions in clinopyroxene, spinel, and rhönite were estimated by stoichiometric following Droop (1987).

In-situ trace element abundances were determined using the same ICP-MS system used in the whole-rock analysis, a Thermo Scientific iCAP Quadrupole equipment coupled with a

laser CETAC LSX-213 G2+. The ablated material was transferred to the ICP-MS in a He flow (0.5 mL/min). Fluence was 5 J/cm^2 with a repetition rate of 12Hz and an ablation spot size (raster mode) between 50 to 30 µm for crystals and 100 to 50 µm for glasses. ICP-MS was monitored for minimal oxide production and U:Th ratio close to 1. For olivine, trace element concentration was determined using NIST SRM 612 for external calibration and the SiO_2 was the internal standard (IS) whereas for glasses, clinopyroxene and amphibole were used NIST SRM 610 and CaO, respectively. IS values were previously determined via EPMA. BIR-1G, BCR-2G, and BHVO-2G were also analyzed as reference glasses of natural compositions to monitor the analytical accuracy and reproducibility. These USGSs glasses lie within an interval of ± 5% of the preferred values from the GeoReM website (Jochum et al., 2005a, 2005b, 2011), see *appendix A.*

For each analysis, the sequence begins with the acquisition of the background signal by 30 s followed by the integrated ablation signal by 50 s. The analytical routine started with NIST glasses and then again after ten analyses.

Data were reduced with the GLITTER 4.5 software package (van Achterbergh et al., 1999) to process the raw data of signal intensity versus time and thus determinate the concentration, analytical errors (1σ) and detection limits.

The isotopes measured for olivine were: ^{7}Li, ^{23}Na, ^{25}Mg, ^{27}Al, ^{29}Si, ^{31}P, ^{42}Ca, ^{45}Sc, ^{49}Ti, ^{51}V, ^{52}Cr, ^{55}Mn, ^{59}Co, ^{60}Ni, ^{63}Cu, ^{66}Zn, ^{85}Rb, ^{88}Sr, ^{89}Y, ^{90}Zr, ^{93}Nb, ^{133}Cs, ^{137}Ba, ^{139}La, ^{140}Ce, ^{141}Pr, ^{143}Nd, ^{147}Sm, ^{151}Eu, ^{157}Gd, ^{159}Tb, ^{163}Dy, ^{165}Ho, ^{166}Er, ^{169}Tm, ^{173}Yb, ^{175}Lu, ^{179}Hf, ^{181}Ta, ^{208}Pb, ^{232}Th, ^{238}U having a dwell time of 20 ms, except for REE with 30 ms.

The isotopes measured for glasses, clinopyroxene and amphibole were: ^{7}Li, ^{9}Be,^{11}B, ^{25}Mg, ^{28}Si, ^{29}Si, ^{31}P, ^{39}K, ^{42}Ca, ^{45}Sc, ^{49}Ti, ^{51}V, ^{52}Cr, ^{55}Mn, ^{59}Co, ^{60}Ni, ^{65}Cu, ^{66}Zn, ^{71}Ga, ^{85}Rb, ^{88}Sr, ^{89}Y, ^{90}Zr, ^{93}Nb, ^{95}Mo, ^{118}Sn, ^{121}Sb, ^{133}Cs, ^{137}Ba, ^{139}La, ^{140}Ce, ^{141}Pr, ^{143}Nd, ^{147}Sm, ^{151}Eu, ^{157}Gd, ^{159}Tb, ^{163}Dy, ^{165}Ho, ^{166}Er, ^{169}Tm, ^{173}Yb, ^{175}Lu, ^{179}Hf, ^{181}Ta, ^{206}Pb, ^{207}Pb, ^{208}Pb, ^{232}Th, ^{238}U having a dwell time of 20 ms.

Table 2-1. Analytical setup used for WDS analyses of minerals from starting materials.

Element	Crystal	Olivine		Pyroxene		Spinel		Feldspar	
		Peak count time (s)	Standard	Peak count time (s)	Standard	Peak count time (s)	Standard	Peak count time (s)	Standard
Si	TAP	10	Diopside	10	Chromium augite	10	San Carlos olivine	10	Anorthoclase
Al		20	Anorthite	15	Chromium augite	10	Gahnite	15	Anorthoclase
Fe	LIFL	10	Fayalite	10	Fayalite	10	Magnetite	10	Fayalite
Mn		40	Fayalite	60	Fayalite	40	Fayalite	40	Fayalite
Ni		50	Corning Glass IR-X			50	Corning Glass IR-X		
Ca	PETJ	20	Wollastonite	15	Wollastonite	20	Wollastonite	10	Wollastonite
Sr*								40	Strontianite
K		10	Orthoclase	20	Orthoclase	10	Orthoclase	10	Orthoclase
Nb*						50	Ilmenite		
Ti	LIFL	10	Rutile	60	Rutile	10	Rutile	10	Rutile
Ba*								30	Benitoite
Cr		10	Chromite	60	Chromite	50	Chromite		
Zn						50	Willemite		
Na	TAPH	20	Albite	10	Albite	10	Albite	10	Albite
Mg		5	San Carlos Olivine	20	Diopside	20	Spinel	10	Diopside

*Lα X-ray

Table 2-2 Analytical setup used for WDS analyses of crystalline phases from experimental products.

Element	Crystal	Olivine		Pyroxene and Rhönite		Spinel		Feldspar		Mica	
		Peak count time (s)	Standard	Peak count time (s)	Standard	Peak count time (s)	Standard	Peak count time (s)	Standard	Peak count time (s)	Standard
Si	TAP	10	San Carlos olivine	10	Kakanui augite	10	San Carlos olivine	10	Anorthoclase	10	Diopside
Al		20	Anorthite	20	Anorthite	10	Gahnite	10	Anorthoclase	15	Anorthite
Fe	LIFL	10	Springwater olivine	10	Springwater olivine	10	Magnetite	20	Fayalite	10	Springwater olivine
Mn		40	Fayalite	30	Fayalite	40	Fayalite	20	Fayalite	20	Fayalite
Ni		50	Corning Glass IR-X	50	Corning Glass IR-X	50	Corning Glass IR-X			50	Corning Glass IR-X
Zn										50	Willemite
Cl										10	Sodalite
Ca	PETJ	20	Wollastonite	15	Wollastonite	20	Wollastonite	10	Wollastonite	20	Wollastonite
Sr*								50	Strontianite		
K		10	Orthoclase	20	Orthoclase	10	Orthoclase	10	Orthoclase	10	Orthoclase
Nb*						50	Ilmenite				
Ti	LIFL	10	Rutile	30	Rutile	10	Rutile	10	Rutile	10	Rutile
Ba*								50	Benitoite	50	Benitoite
Cr		50	Chromite	50	Chromite	50	Chromite			50	Chromite
Zn		10	Willemite	50	Willemite	50	Willemite				
F										10	Fluorapatite
Na	TAPH	20	Albite	10	Albite	10	Albite	10	Albite	10	Albite
Mg		10	San Carlos Olivine	20	Diopside	20	Spinel	10	Diopside	10	Diopside

*Lα X-ray

Table 2-3. Analytical setup used for WDS analyses of glasses from experimental products.

Element	Crystal	Glass	
		Peak count time (s)	Standard
Na	TAP	5	Albite
Al		5	Basaltic glass VG-2
K	PETL	5	orthoclase
Ca		5	Basaltic glass VG-2
S		10	Meionite
Si	PETJ	5	Basaltic glass A-99
Cl		10	Sodalite
P		10	Fluorapatite
Sr*		20	Strontianite
Fe	LIFL	5	Basaltic glass A-99
Mn		20	Fayalite
Ti		10	Rutile
Ba*		20	Benitoite
F	TAPH	5	Fluorapatite
Mg		10	Basaltic glass VG-2

*Lα X-ray

2.3.Experimental techniques

The starting material was previously dried at 100°C / 24h before mounting the experimental charges. One-atmosphere and low- to high-pressure experiments were carried out with a vertical tube furnace and a piston-cylinder, respectively. In both cases, after charge load, the temperature was increased at 5 °C/ min until 100 °C above the *liquidus* temperature, evaluated with the rhyolite-MELTS spreadsheet (Gualda and Ghiorso, 2015). Then, this temperature was held for 1h (glassing step) and later the temperature was lowered at 1°C/min until run temperature for 48h (*Figure 2.1*). The run time was chosen following Suzuki et al. (2012) to approach equilibrium. After the running step, the experiments were quenched. The obtained capsules and pellets were mounted in epoxy resin and polished to expose their cores for analytical purposes. 18 experiments were carried out under low- to high-pressure and other 33 under one-atmosphere conditions.

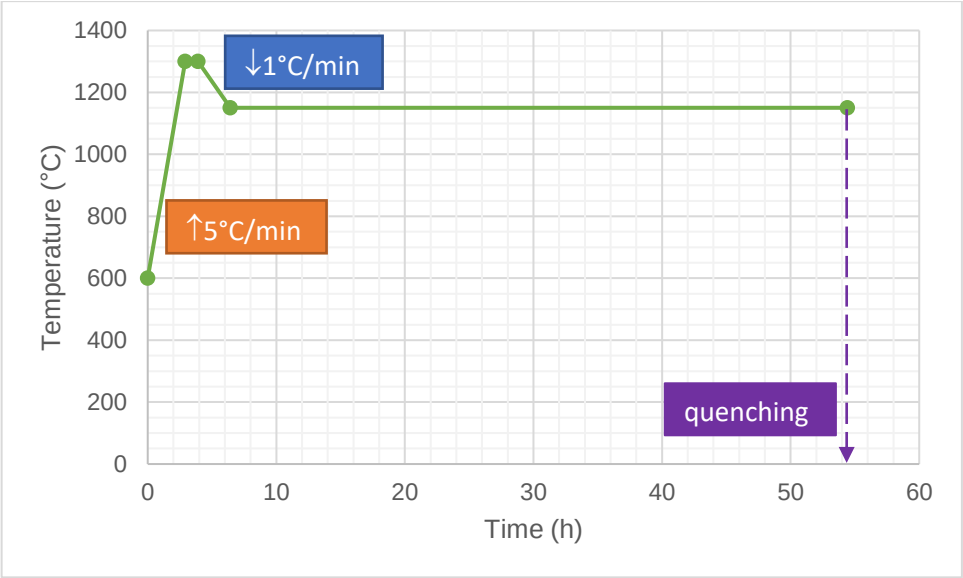

Figure 2.1. Temperature steps during each experimental run performed in the high-temperature vertical furnace. In the figure, the heating (orange) and cooling (blue) rates are indicated.

2.3.1. One-atmosphere experiments

Experiments under atmospheric pressure and anhydrous conditions were performed in a high-temperature vertical tube furnace GERO HTRV 70-250/18, which is coupled to Ar, CO, CO_2, O2, and SO_2 gas mixing system with Aalborg AFC26 mass flow controllers. The accuracy in oxygen fugacity is 0.1 log-bar units inside the furnace (e.g., Mallmann et al., 2014). Oxygen fugacity is controlled by gas mixtures (Kress et al., 2004) and checked before starting the experimental work with a $SIRO_2$ C700+ solid zirconia electrolyte oxygen sensor.

The charges for HTRV equipment were arranged using the wire-loop technique (Presnall and Brenner, 1974), in which a powder starting sample is mixed with polyethylene gel prepared from polyethylene oxide and water until sludge is achieved. It was mounted on Pt-Fe wire alloy, forming a "pearl", which was suspended in a Pt “chandelier” (e.g. Mallmann and O’Neill, 2009) and then placed in the hotspot of the furnace, where the thermal gradient is <1 °C (*Figure 2.2*). This hot zone was checked before experiments with a temperature vertical profile inside of the furnace with a B-type thermocouple.

Figure 2.2. (a) High-temperature vertical tube furnace GERO HTRV 70-250/18 was used in this study. (b) Alumina spindle (c) Pellets mounted on Pt metal wire before they insert into a high-temperature vertical furnace.

The Pt wire was pre-saturated with iron (~9 wt.%) to minimize iron loss from the starting material to the Pt wire-loop as a consequence of the interaction between both high temperatures during the experiment and reduced conditions. This effect is caused by the solid solution between Fe and Pt, where a PtFe alloy is formed and the excess of O_2 is liberated. We followed the electroplating/annealing procedures described by Grove (1981). The electroplating was carried out under constant current (10mA) using a computer-controlled

Autolab PGSTAT128n potentiostat at the Electrochemical Sensors and Electroanalytical Methods Laboratory of the Institute of Chemistry, University of São Paulo. The Pt wire was immersed in a supersaturated solution of ferrous sulfate (FeSO4) and the electrodeposition was achieved by applying a fixed and sufficiently negative potential enabling in situ metallic electrodeposition, following the reaction:

$$FeSO_4+2e^-+2H^+ \rightarrow Fe^0+H_2SO_4 \text{ (Equation 2.1)}$$

Then, the annealing was performed in HTRV equipment under 1200 °C and close to the iron-wüstite (IW) buffer for 48h to produce a homogenous alloy.

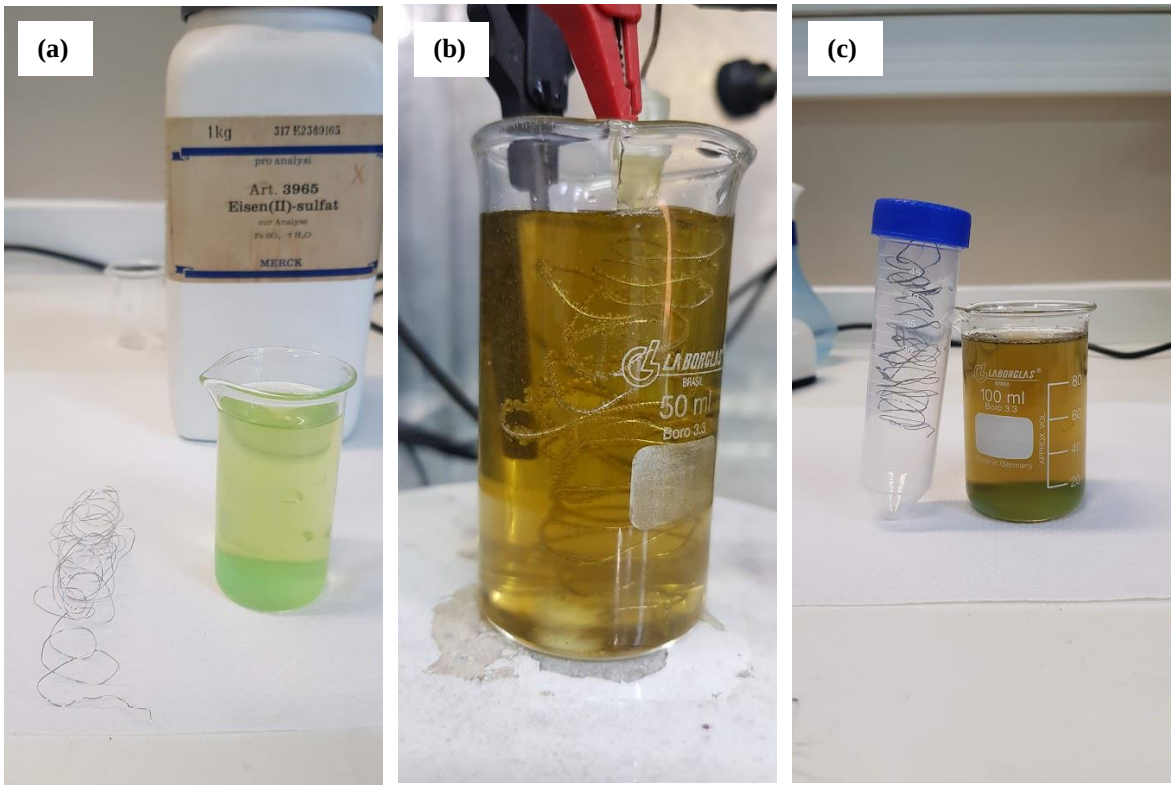

Figure 2.3. The electroplating procedure. (a) Pt wire and $FeSO_4$ before the procedure. (b) Pt wire was immersed in the $FeSO_4$ solution. Note the color change in the solution and the burble. (c) Pt wire with iron on its surface.

The experiments were performed at five oxygen fugacities relative to quartz-fayalite-magnetite buffer (QFM) from reduced to oxidized conditions (ΔQFM-2 to ΔQFM+2) controlled in glassing and running steps. After the time run, the products were quenched by mechanical release and then fell into distilled and deionized H_2O at room temperature. A summary of these experimental conditions is shown in Table *2-4*.

Table 2-4. Conditions of experiments run under one-atmosphere pressure.

#	ID		Conditions			
	Basanite	Tephrite	T (°C)	ΔQFM	CO (sccm)	CO_2 (sccm)
1	D1, B1*	C1, A1*	1150	2	8.0x10	86.0x200
2	Q2		1150	1	26.6x10	90.0x200
3	B2	A2*	1150	0	47.0x10	50.0x200
4	Q1		1150	-1	13.3x200	90x200
5	D2, D4*	A3*	1150	-2	23.5x200	50.0x200
6	R1	Q3	1100	2	7.3x10	88.0x200
7	T1	T2	1100	1	20.0x10	76.0x200
8	V1	V2	1100	0	36.0.x10	44.0x200
9	Z1	Y1	1100	-1	10.0x200	76.0x200
10	U1	U2	1100	-2	21.5x200	53x200
11	O2	N3	1050	2	6.5x10	90x200
12	Z2	Y2	1050	1	20.0x10	87.0x200
13	O3	N2	1050	0	65x10	90x200
14	X1	X2	1050	-1	10.0x200	87.0x200
15	P1	N1	1050	-2	19.5x200	54x200
16	ZA1, ZA2*		1000	0	28x10	45x200

*Non-doped samples. sccm=standard cubic centimeter per minute.

2.3.2. Low- to high-pressure experiments

Experiments under low (0.5 GPa) to high (1.0 to 2.0 GPa) pressure were carried out with an end-loaded Bristol-type piston-cylinder (PC) apparatus, using ¾'' and ½'' assembly cells composed of MgO, graphite, pyrex glass and NaCl, which was wrapped in Pb-foil (*e.g.*, Vlach et al., 2019a). However, under low pressure, temperatures > *ca*. 1100°C cannot be achieved with the original design of the ¾''assembly. To overcome this, the ¾'' assembly was slightly modified by combining the crushable MgO, graphite, and pyrex glass from the ½'' assembly, with a thicker NaCl sleeve, compatible with the conventional ¾'' assembly and the other components (*Figure 4.2*). This arrangement requires great caution to assemble components and conduct experiments to avoid failure.

The starting material was packed into a graphite inner capsule (2.0 mm inner diameter) covered with a graphite lid, which in turn was placed in a 3.0 mm (inner diameter) Pt outer capsule to avoid Fe loss during the experiments (e.g., Médard et al., 2008; Laporte et al., 2014; Armstrong et al., 2015). This arrangement imposes redox conditions close to the CCO buffer. The capsules follow the trashcan design, and the base and top lids were welded with a Lampert PUK U3 high-precision welding machine (see *Figure 2.4*). The temperature of the experiments was set up and monitored using a B-type thermocouple ($Pt_{94}Rh_{06}$-$Pt_{70}Rh_{30}$) and a Eurotherm 2404 PID controller. Piston-cylinder pressures were calibrated following Vlach et

al. (2019a) and McDade et al. (2002) for the low to high ranges, respectively. During experiments the pressure was applied following the hot-piston-in technique (Johannes et al., 1971); to maintain the desired pressure during run time, minor pumping was occasionally needed. The charges were quenched to room temperature by cutting off the power supply.

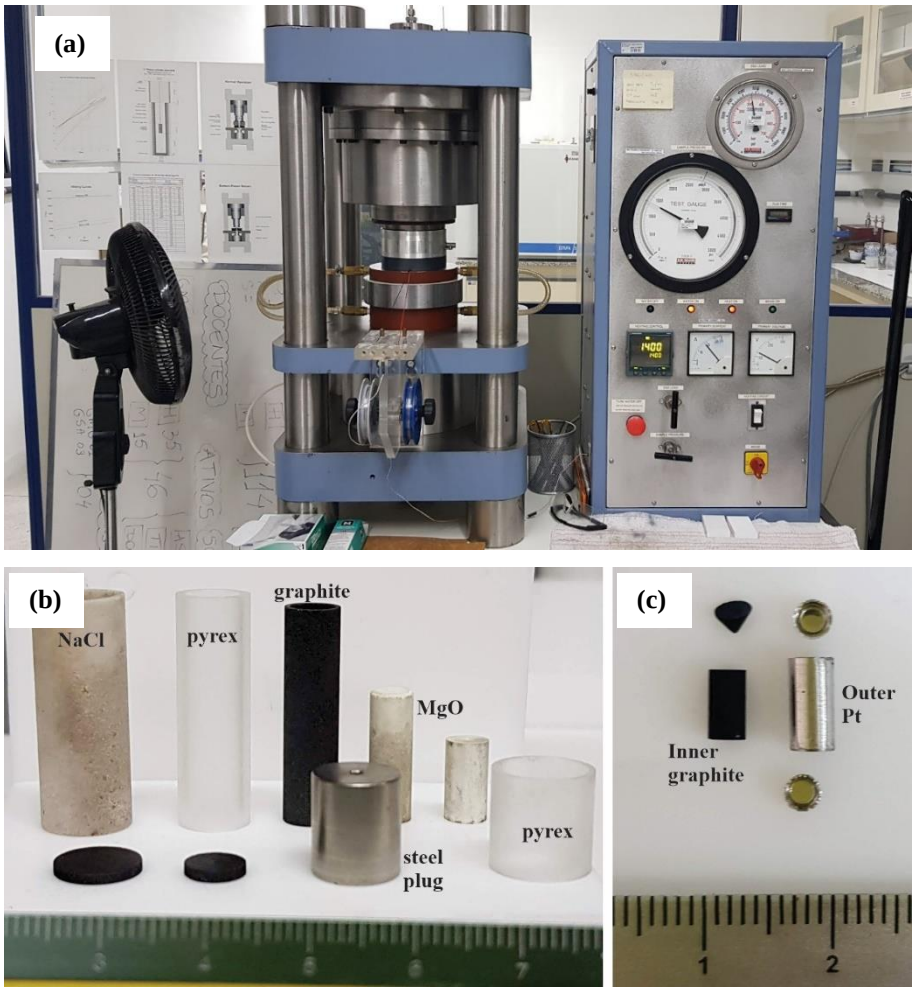

Figure 2.4. (a) The End-loaded Bristol-type piston-cylinder apparatus used in this study. (b) Components of the ½'' assembly for high-pressure and temperature experiments. (c) Pt-graphite capsule.

A summary of the conditions of experiments performed from low- to high-pressure is presented in *Table 2-5*.

Table 2-5. Conditions of experiments run from low- to high-pressure.

#	ID	Assembly	Conditions	
			P (GPa)	T (°C)
Basanite				
1	I3	½''	2.0	1360
2	K1	½''	2.0	1250
3	G2	½''	1.5	1300
4	S2	½''	1.5	1200
5	G3	½''	1.0	1240
6	E1, J1*	½''	1.0	1200
7	L1*#	½''	1.0	1050
8	E2, E3*	¾'' mod.	0.5	1195
Tephrite				
9	H1	½''	2.0	1360
10	K2	½''	2.0	1250
11	H2	½''	1.5	1300
12	S1	½''	1.5	1200
13	H3	½''	1.0	1240
14	K3	½''	1.0	1180
15	F1	¾'' mod.	0.5	1180

**Non-doped samples. # It was added 10 wt.% of H_2O

2.4. References

van Achterbergh, E., Ryan, C.G., and Griffin, W.L., 1999, GLITTER: On-line interactive data reduction for the laser ablation inductively coupled plasma mass spectrometry microprobe, in Ninth Annual VM Goldschmidt Conference, p. 7215.

Armstrong, L.S., Hirschmann, M.M., Stanley, B.D., Falksen, E.G., and Jacobsen, S.D., 2015, Speciation and solubility of reduced C-O-H-N volatiles in mafic melt: Implications for volcanism, atmospheric evolution, and deep volatile cycles in the terrestrial planets: Geochimica et Cosmochimica Acta, v. 171, p. 283–302, doi:10.1016/j.gca.2015.07.007.

Droop, G.T.R., 1987, A General Equation for Estimating Fe3+ Concentrations in Ferromagnesian Silicates and Oxides from Microprobe Analyses, Using Stoichiometric Criteria: Mineralogical Magazine, v. 51, p. 431–435, doi:10.1180/minmag.1987.051.361.10.

Grove, T.L., 1981, Use of FePt alloys to eliminate the iron loss problem in 1 atmosphere gas mixing experiments: Theoretical and practical considerations: Contributions to Mineralogy and Petrology, v. 78, p. 298–304, doi:10.1007/BF00398924.

Gualda, G.A.R., and Ghiorso, M.S., 2015, MELTS_Excel: A Microsoft Excel-based MELTS interface for research and teaching of magma properties and evolution: Geochemistry, Geophysics, Geosystems, v. 16, p. 315–324, doi:10.1002/2014GC005545.

Jochum, K.P. et al., 2011, Determination of reference values for NIST SRM 610-617 glasses following ISO guidelines: Geostandards and Geoanalytical Research, v. 35, p. 397–429, doi:10.1111/j.1751-908X.2011.00120.x.

Jochum, K.P., Nohl, U., Herwig, K., Lammel, E., Stoll, B., and Hofmann, A.W., 2005a, GeoReM: A new geochemical database for reference materials and isotopic standards: Geostandards and Geoanalytical Research, v. 29, p. 333–338, doi:10.1111/j.1751-908x.2005.tb00904.x.

Jochum, K.P., Willbold, M., Raczek, I., Stoll, B., and Herwig, K., 2005b, Chemical characterisation of the USGS reference glasses GSA-1G, GSC-1G, GSD-1G, GSE-1G, BCR-2G, BHVO-2G and BIR-1G using EPMA, ID-TIMS, ID-ICP-MS and LA-ICP-MS: Geostandards and Geoanalytical Research, v. 29, p. 285–302, doi:10.1111/j.1751-908x.2005.tb00901.x.

Johannes, W., Bell, P.M., Mao, H.K., Boettcher, A.L., Chipman, D.W., Hays, J.F., Newton, R.C., and Seifert, F., 1971, An interlaboratory comparison of piston-cylinder pressure calibration using the albite-breakdown reaction: Contributions to Mineralogy and Petrology, v. 32, p. 24–38, doi:10.1007/BF00372231.

Kress, V.C., Ghiorso, M.S., and Lastuka, C., 2004, Microsoft EXCEL spreadsheet-based program for calculating equilibrium gas speciation in the C-O-H-S-Cl-F system: Computers and Geosciences, v. 30, p. 211–214, doi:10.1016/j.cageo.2003.10.006.

Laporte, D., Lambart, S., Schiano, P., and Ottolini, L., 2014, Experimental derivation of nepheline syenite and phonolite liquids by partial melting of upper mantle peridotites: Earth and Planetary Science Letters, v. 404, p. 319–331, doi:10.1016/j.epsl.2014.08.002.

Mallmann, G., Fonseca, R.O.C., and Silva, A.B., 2014, An experimental study of the partitioning of trace elements between rutile and silicate melt as a function of oxygen fugacity: Anais da Academia Brasileira de Ciencias, v. 86, p. 1609–1629, doi:10.1590/0001-3765201420140014.

Mallmann, G., and O'Neill, H.S.C., 2009, The crystal/melt partitioning of V during mantle melting as a function of oxygen fugacity compared with some other elements (Al, P, Ca, Sc, Ti, Cr, Fe, Ga, Y, Zr and Nb): Journal of Petrology, v. 50, p. 1765–1794, doi:10.1093/petrology/egp053.

McDade, P., Wood, B.J., van Westrenen, W., Brooker, R., Gudmundsson, G., Soulard, H., Najorka, J., and Blundy, J., 2002, Pressure corrections for a selection of piston-cylinder cell assemblies: Mineralogical Magazine, v. 66, p. 1021–1028, doi:10.1180/0026461026660074.

McGuire, A.., Francis, C.., and Dyar, M.., 1992, Mineral standards for electron micrprobe analysis of oxygen: American Mineralogist, v. 77, p. 1087–1091.

Médard, E., McCammon, C.A., Barr, J.A., and Grove, T.L., 2008, Oxygen fugacity, temperature reproducibility, and H2O contents of nominally anhydrous piston-cylinder experiments using graphite capsules: American Mineralogist, v. 93, p. 1838–1844, doi:10.2138/am.2008.2842.

Mori, P.E., Reeves, S., Correia, C.T., and Haukka, M., 1999, Development oof a fused glass disc XRF facility and comparison with the pressed powder pellet technique at Instituto de Geociencias, Sao Paulo University: Revista Brasileira de Geociencias, v. 29, p. 441–6, http://inis.iaea.org/Search/search.aspx?orig_q=RN:32037921 (accessed October 2016).

Navarro, M.S., Andrade, S., Ulbrich, H., Gomes, C.B., and Girardi, V.A.V., 2008, The Direct Determination of Rare Earth Elements in Basaltic and Related Rocks using ICP-MS: Testing the

Efficiency of Microwave Oven Sample Decomposition Procedures: Geostandards and Geoanalytical Research, v. 32, p. 167–180, doi:10.1111/j.1751-908X.2008.00840.x.

Presnall, D.C., and Brenner, N.L., 1974, A method for studying iron silicate liquids under reducing conditions with negligible iron loss: Geochimica et Cosmochimica Acta, v. 38, doi:10.1016/0016-7037(74)90161-6.

Suzuki, T., Hirata, T., Yokoyama, T.D., Imai, T., and Takahashi, E., 2012, Pressure effect on element partitioning between minerals and silicate melt: Melting experiments on basalt up to 20GPa: Physics of the Earth and Planetary Interiors, v. 208–209, p. 59–73, doi:10.1016/j.pepi.2012.07.008.

Vlach, S.R.F., Salazar-Naranjo, A.F., Torres-Corredor, J.S., De Carvalho, P.R., and Mallmann, G., 2019, Calibration of high-temperature furnace assemblies for experiments between 200 and 600 MPa with end-loaded piston-cylinder apparatuses: Brazilian Journal of Geology, v. 49, doi:10.1590/2317-488920192018090.

6. FINAL REMARKS

Crystallization experiments of basanitic and tephritic charges under one-atmospheric pressure at reducing to oxidizing conditions ($-2 \leq \Delta QFM \leq 2$) and under low- to high-pressure at reducing conditions (CCO) provided the following: (1) new constraints for the evolution of the alkali ultrabasic to intermediate magmas and their mineral assemblage; (2) equilibrium criteria between mafic silicate minerals (olivine and clinopyroxene) and alkali melts; (3) thermobarometry and; (4) trace element partitioning elements between titanian Ca-clinopyroxene and alkali melts.

1. The liquid lines of descent are sodic and strongly SiO_2-undersaturated for basanite and sodic-potassic/potassic and weakly SiO_2-undersaturated to SiO_2-saturated for tephrite, both under 100 kPa and temperatures between 1150-1000 °C. Under low- to high-pressures, the evolution trend is marked by the increase in the total alkalis with minor variations in SiO_2 contents. The crystallization sequence in basanite starts with olivine, followed by clinopyroxene, and continued with rhönite under 100 kPa or biotite under 1.5 GPa. Clinopyroxene is the *liquidus* phase in tephrite, followed by plagioclase, and subsequently by olivine, the latter only under reduced conditions.

2. The iron-magnesium exchange between mafic silicate minerals and alkali melts was 0.29±0.02 for olivine and 0.26±0.02 for clinopyroxene, which are values slightly lower than in tholeiitic systems.
3. Tracking the *liquidus* temperature and crystallization pressure in alkali ultrabasic to intermediate compositions is possible using the thermobarometric equations that were improved in this thesis. These formulations are based on MgO-in-melt and clinopyroxene composition (Na, Ti, and Fe^{3+} cations), respectively.

4. The trivalent cations that are allocated into M1 site in clinopyroxene are principally Al, Sc, and Ga under reduced conditions or Al, Sc, V, and Ga under oxidizing conditions. Cr should be considered as part of divalent FRTMs, besides it is strongly compatible with clinopyroxene, in the fO_2 tested in this investigation. Both fO_2 and temperature have a strong influence on V partitioning in clinopyroxene.
5. P-T and fO_2 also control the partitioning behavior of REE and HFSE, but the allocation of these elements is governed by Tschermak-type substitution and, at the

same time, the behavior follows the evolutional path of clinopyroxene, where ferroan diopside is more compatible than Mg-rich augite.

6. The available models to predict the REE partitioning between clinopyroxene and silicate melts do not reproduce the negative correlation between D_0^{REE} and pressure. On the other hand, Wood and Blundy´s (1997) model reproduces very well D_0^{REE} of experimental data at 100 kPa and both models, Wood and Blundy (1997) and Sun and Liang (2012), predict satisfactorily r_0^{REE} and E.
7. Finally, this investigation provides a new experimental dataset for trace element partition coefficients between titanian Ca-clinopyroxene and alkali ultrabasic to intermediate melts, representative of the two main magma series mentioned above. Furthermore, this information may help geoscientists to better understand the formation and differentiation processes of alkali igneous rocks with future petrological and geochemical modeling.